Large Rashba spin splittings in bulk and monolayer of BiAs

Muhammad Zubair [1,2,*] Igor Evangelista [2] Shoaib Khalid [3] Bharat Medasani [3] and Anderson Janotti [2,†]
[1] Department of Physics and Astronomy, University of Delaware, Newark, Delaware 19716, USA
[2] Department of Materials Science and Engineering, University of Delaware, Newark, Delaware 19716, USA
[3] Princeton Plasma Physics Laboratory, P.O. Box 451, Princeton, New Jersey 08543, USA

(Received 26 October 2023; accepted 1 May 2024; published 20 May 2024)

There is great interest in developing new materials with Rashba split bands near the Fermi level for spintronics. Using first-principles calculations, we predict BiAs as a semiconductor with large Rashba splitting in bulk and monolayer forms. Bulk BiAs has a layered crystal structure with two atoms in a rhombohedral primitive cell, derived from the structure of the parent Bi and As elemental phases. It is a narrow band gap semiconductor, and it shows a combination of Rashba and Dresselhaus spin splitting with a characteristic spin texture around the L point in the Brillouin zone of the hexagonal conventional unit cell. It has sizable Rashba energies and Rashba coupling constants in the valence and conduction bands at the band edges. The 2D monolayer of BiAs has a much larger band gap at Γ, with a circular spin texture characteristic of a pure Rashba effect. The Rashba energy and Rashba coupling constant of monolayer BiAs are large compared to other known 2D materials and rapidly increase under biaxial tensile strain.

DOI: 10.1103/PhysRevMaterials.8.054604

I. INTRODUCTION

Rashba-type spin-orbit coupling (SOC) plays a crucial role in spintronics, [1–8] as it facilitates the generation, detection, and manipulation of spin current without external magnetic field [9]. Three parameters quantify the strength of the Rashba effect, namely the Rashba energy (E_R), the Rashba momentum (K_o), and the Rashba coupling constant (α_R) [10], and these can be tuned by an external electric field [9]. Basically, spin-degenerate bands split into two parabolic bands, e.g., spin up and spin down, with the Rashba Hamiltonian given by $H_R = \alpha_R(\hat{z} \times \mathbf{k}) \cdot \sigma$. The band dispersion can be described by $E(k) = (\hbar^2 k^2/2m) \pm \alpha_R k$, where m is the effective mass of the electron or hole. This type of SOC is usually caused by a lack of inversion symmetry due to a confining potential associated with an interface or surface [10–12], whereas the lack of inversion symmetry in the bulk is associated with the Dresselhaus type of spin-orbit coupling [13,14]. In many materials, the Rashba and Dresselhaus SOC effects are coupled, resulting in spin-splitting anisotropy that causes interesting phenomena such as the spin helix and long spin relaxation times observed in GaAs [1–8,15].

Two-dimensional (2D) semiconductors with strong Rashba effects are great candidate materials for spintronic devices such as spin field-effect transistors [16]. A 2D Rashba semiconductor interfaced with an s-wave superconductor under broken time-reversal symmetry could be used to build topological heterostructures to detect Majorana fermions [17–19] for quantum information in quantum computation [20,21]. Among all 2D materials with strong SOC, Bi, BiSb, and $Bi_{1-x}Sb_x$ have received special attention in the investigation of the Rashba effect [22] and nontrivial topological electronic states [23–27]. Bi forms a layered structure and is semimetallic with a small overlap of valence and conduction bands [23,26]. A peculiar Rashba-type band splitting was observed on Bi(111) surface by high-resolution spin- and angle-resolved photoemission spectroscopy using Si(111) as substrate [28]. Bulk BiSb also forms a layered structure and density functional theory calculations reveal an indirect band gap of E_g= 160 meV, with an interesting band splitting, attributed to the SOC, at the L point in the hexagonal Brillouin zone [29], while nontrivial topological states were observed in $Bi_{1-x}Sb_x$ for specific composition range [23–25].

As research continues to explore novel materials for advancing spintronics, bismuth arsenide (BiAs) emerges as a natural extension to Bi and BiSb, with an expected larger band gap and larger bandwidth due to shorter Bi-As bond length while still retaining a strong spin-orbit coupling due to Bi. However, information on BiAs is lacking in the literature as it has not yet been synthesized. In the present study, we use first-principles calculations to predict the structural and electronic properties of BiAs. We find that BiAs also form a layered structure, with a rhombohedral R3m space group, as shown in Figs. 1(a) and 1(b), similar to BiSb [29] and derived from that of Bi. Our results show that bulk BiAs is a semiconductor with a small and indirect band gap, and displays a combination of Rashba and Dresselhaus SOC splitting near the L point in the Brillouin zone of the hexagonal unit cell. In the monolayer form [Fig. 1(c)], BiAs has a much larger and direct band gap with a pure Rashba splitting at Γ. The strength of the Rashba effect and the fact that it can be tuned by applying biaxial or uniaxial strain make this material of interest for optoelectronics and spintronics.

*mzubair@udel.edu
†janotti@udel.edu

 ©2024 American Physical Society

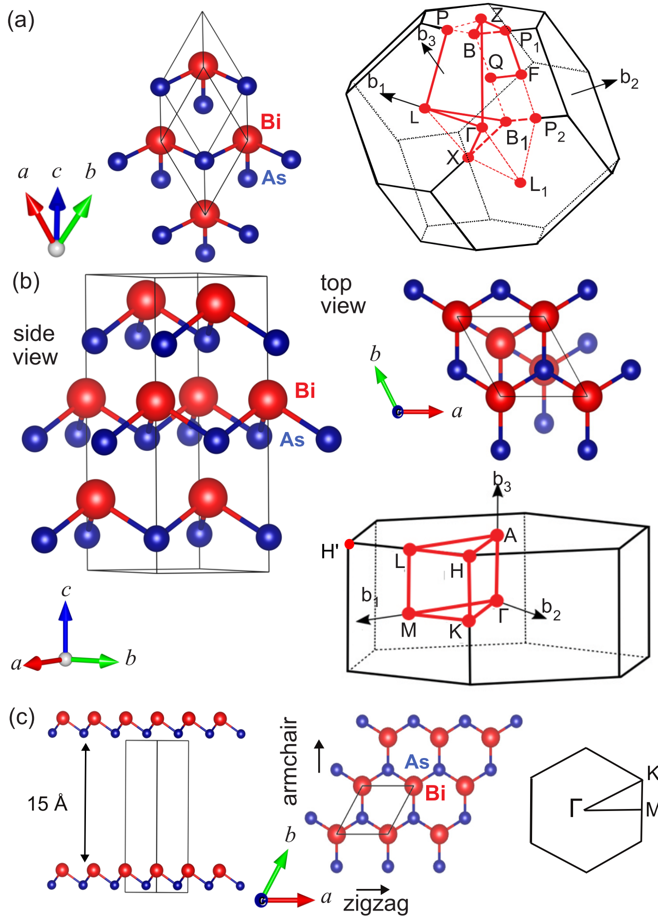

FIG. 1. Layered crystal structure of bulk BiAs, space group R3m, represented by (a) a rhombohedral primitive cell containing two atoms and (b) a conventional hexagonal unit cell containing six atoms (side and top views). (c) Supercell used in the calculations of the monolayer BiAs (side and top views), with armchair and zigzag directions indicated. The corresponding Brillouin zones with high-symmetry points and directions are also shown on the right.

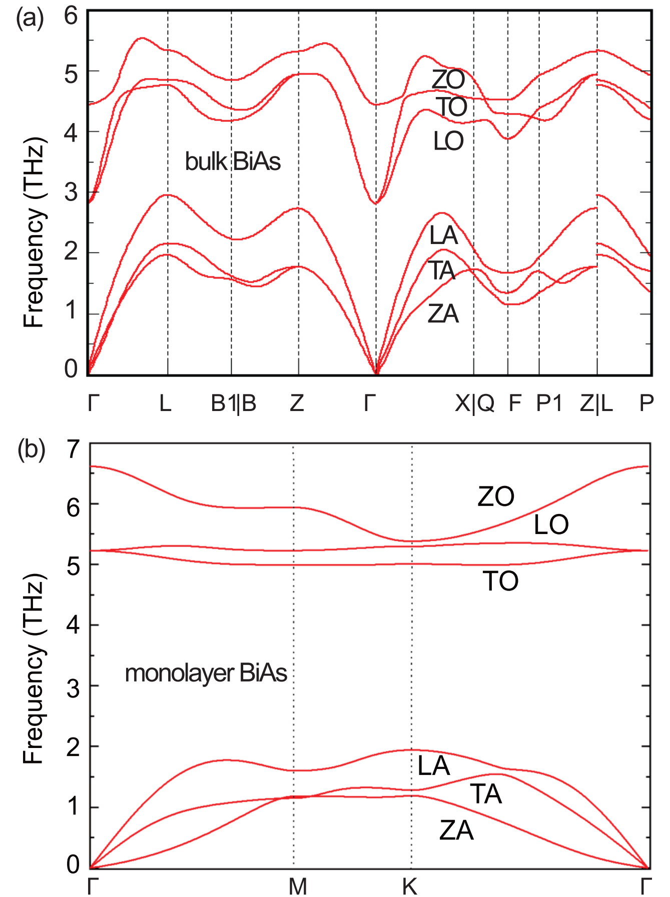

FIG. 2. Calculated phonon dispersion along the high-symmetry lines for (a) the rhombohedral R3m structure of the bulk BiAs and (b) monolayer BiAs.

II. COMPUTATIONAL APPROACH

Density functional theory (DFT) [30,31] calculations as implemented in the VASP code [32] were employed to investigate the structural and electronic properties of BiAs. The interactions between the valence electrons and ions were treated using projector augmented-wave (PAW) potentials [33] that include five valence electrons for Bi ($6s^26p^3$) and five for As ($4s^24p^3$). We used the generalized gradient approximation of Perdew, Burke, and Ernzerhoff (PBE) [34] for determining equilibrium structures and the electronic structure. We also used the screened hybrid functional of Heyd-Scuseria-Ernzerhof (HSE06) [35,36] for estimating band gaps based on the structures obtained using the PBE functional. Plane-wave basis set with a cutoff of 500 eV and an $8\times8\times8$ k mesh for the integrations over the Brillouin zone of the two-atom rhombohedral primitive cell and equivalent k-mesh density for the six-atom hexagonal unit cell were employed. Convergence criteria for the total energy and the forces on each atom were set to 10^{-6} eV and 10^{-4} eV/Å, respectively.

Electronic band structure calculations were performed including the effects of SOC and without SOC for comparison. In the case of the monolayer BiAs, a supercell with a vacuum layer thickness of 15 Å along the c axis was used to minimize interactions between periodic images [Fig. 1(c)]. To investigate the effect of in-plane biaxial strain for monolayer BiAs, we varied the a and b lattice vectors from −6% (compression) to +6% (expansion) while performing relaxation of all the atomic positions. In the case of uniaxial strain, we considered the armchair and zigzag directions [Fig. 1(c)]; the length of the cell along a given direction is fixed while relaxing the length in the perpendicular direction and all the atomic positions. Note that the hexagonal Brillouin zone will be slightly distorted in these cases. Finally, the PYPROCAR code was used to calculate the constant energy contour plots of the spin texture [37].

III. RESULTS AND DISCUSSION

We first determined the lowest energy phase of BiAs, carrying out DFT calculations for various possible crystal structures, including rocksalt, rhombohedral, hexagonal boron nitride, body-centered CsCl, and zinc blende. Only the rhombohedral crystal structure (space group R3m) resulted in a negative formation enthalpy, with $\Delta H_f = -40$ meV/atom, which

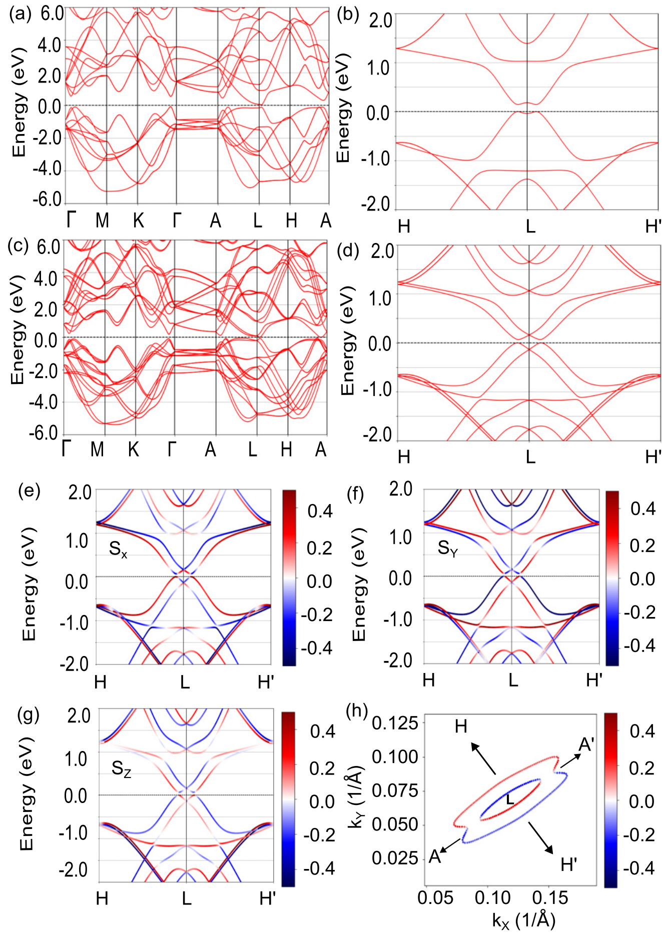

FIG. 3. Electronic band structure of bulk BiAs without SOC (a) along all the main high symmetry directions and (b) focusing on the H-L-H' direction of the hexagonal Brillouin zone. The corresponding band structures with SOC are shown (c) and (d). Spin-resolved band structure for (e) (S_x), (f) (S_y), and (g) (S_z) projections. (h) Spin texture around the L point of the Brillouin zone at 0.2 eV above the Fermi level.

is higher in magnitude than the value of -15 meV/atom reported for BiSb [29]. In this structure, Bi and As atoms are stacked along the (111) direction of the rhombohedral primitive cell containing two atoms [Fig. 1(a)]. The calculated lattice parameters are $a = b = c = 4.318$ Å and $\alpha = \beta = \gamma = 58.3^\circ$. Note that no experimental data is available.

To check the structural stability of BiAs in the rhombohedral phase, phonon calculations using density functional perturbation theory (DFPT) were carried out using the PBE functional. The phonon band structure of bulk BiAs is shown in Fig. 2(a). With two atoms in the primitive cell, BiAs has six phonon branches, three lower-frequency acoustic branches, and three higher-frequency optical branches. From the phonon band structure, the longitudinal acoustic (LA), longitudinal optical (LO), transverse acoustic(TA), transverse optical(TO), and out-of-plane acoustic (ZA), and out-of-plane optical (ZO) modes were identified. It can be clearly seen that there are no negative frequencies in the phonon band structure, indicating that BiAs in the rhombohedral phase is structurally and dynamically stable.

TABLE I. Rashba energy E_R and Rashba coupling constant α_R for BiAs bulk valence (v) and conduction (c) bands, and BiAs monolayer (c). Data for other Bi-containing materials and other established materials are listed for comparison. The last column indicates if the results are from experiments or calculations (Calc.).

Compound	E_R (meV)	α_R(eV Å)	Ref.
BiAs bulk (c)	93	4.35	(present paper)
BiAs bulk (v)	137	5.93	(present paper)
BiAs monolayer (c)	18.6	2.17	(present paper)
BiSb bulk(c)	147	10.43	[29] Calc.
BiSb bulk(v)	66	4.71	[29] Calc.
BiSb monolayer(c)	13	2.3	[43] Calc.
BiTeI	100	3.8	[39] Calc.
BiTeCl	18.45	1.2	[41] Exp.
BiTeBr	<50	<2	[44] Exp.
Bi(111)	14	0.55	[45] Exp.
$BiAlO_3$(R3c)	7.34	0.39	[40] Calc.
$BiAlO_3$(P4mm)	9.4	0.74	[40] Calc.
LiZnSb	21	1.82	[46] Calc.
KMgSb	10	1.82	[46] Calc.
NaZnSb	31	2.58	[46] Calc.
Au(111)	2.1	0.33	[47] Exp.
GeTe	227	4.8	[48] Calc.
SnTe	272	6.8	[49] Calc.
PbI_3	12	1.5	[50] Calc.
SnI_3	11	1.9	[50] Calc.

A. Electronic properties of bulk BiAs

For ease of comparison of the band structures of bulk and monolayer BiAs, we used the conventional hexagonal unit cell containing six atoms (three BiAs bilayers) as shown in Fig. 1(b) along the corresponding Brillouin zone. The lattice parameters for the hexagonal crystal structure are $a = b = 4.207$ Å, $c = 10.712$ Å, and the angles are $\alpha = \beta = 90^\circ$, $\gamma = 120^\circ$. The band structures in the conventional hexagonal unit cell of bulk BiAs, with and without SOC and using the PBE functional, are shown in Fig. 3. The band gap occurs along the H-L direction, closer to L, similar to the results for BiSb [29]. The band gap including SOC is 42 meV. The band structures in Figs. 3(c) and 3(d) show sizable spin splittings around the L point in both valence and conduction bands.

Bahramy *et al.* established three conditions for the existence of a large Rashba effect in bulk: (i) large SOC in an inversion-asymmetric system, (ii) a narrow band gap, and (iii) valence-band maximum (VBM) and conduction-band minimum (CBM) of symmetrically same character [38]. The band structure plotted along the H-L-H' direction displayed in Fig. 3(d) shows that bulk BiAs satisfies these three conditions and consequently exhibits a very large Rashba effect, as seen in the spin-resolved band structure in Figs. 3(e)–3(g). The presence of Rashba spin splitting is attributed to the strong spin-orbit coupling of the Bi atoms. The spin-resolved band structures showing the spin projected on the cartesian coordinates S_x, S_y, and S_z along the H-L-H' direction are shown in Figs. 3(e)–3(g). The results show significant spin density near the valence-band maximum (VBM) and conduction-band minimum (CBM). Spin splitting is observed in all three components of spin, indicating the presence of both Rashba- and

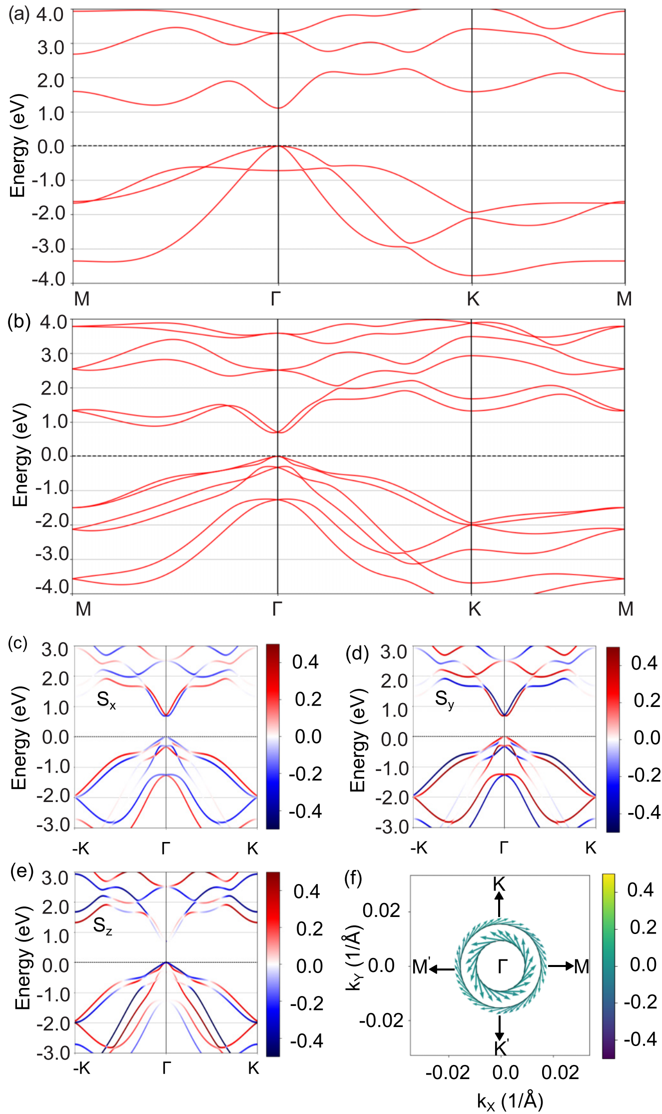

FIG. 4. Electronic band structure of monolayer BiAs along the M-Γ-K-M directions (a), (b) without SOC and with SOC. Spin-resolved band structure for (c) (S_x), (d) (S_y), and (e) (S_z) projections. (f) Spin texture around the Γ point of the Brillouin zone at 0.75 eV above Fermi level.

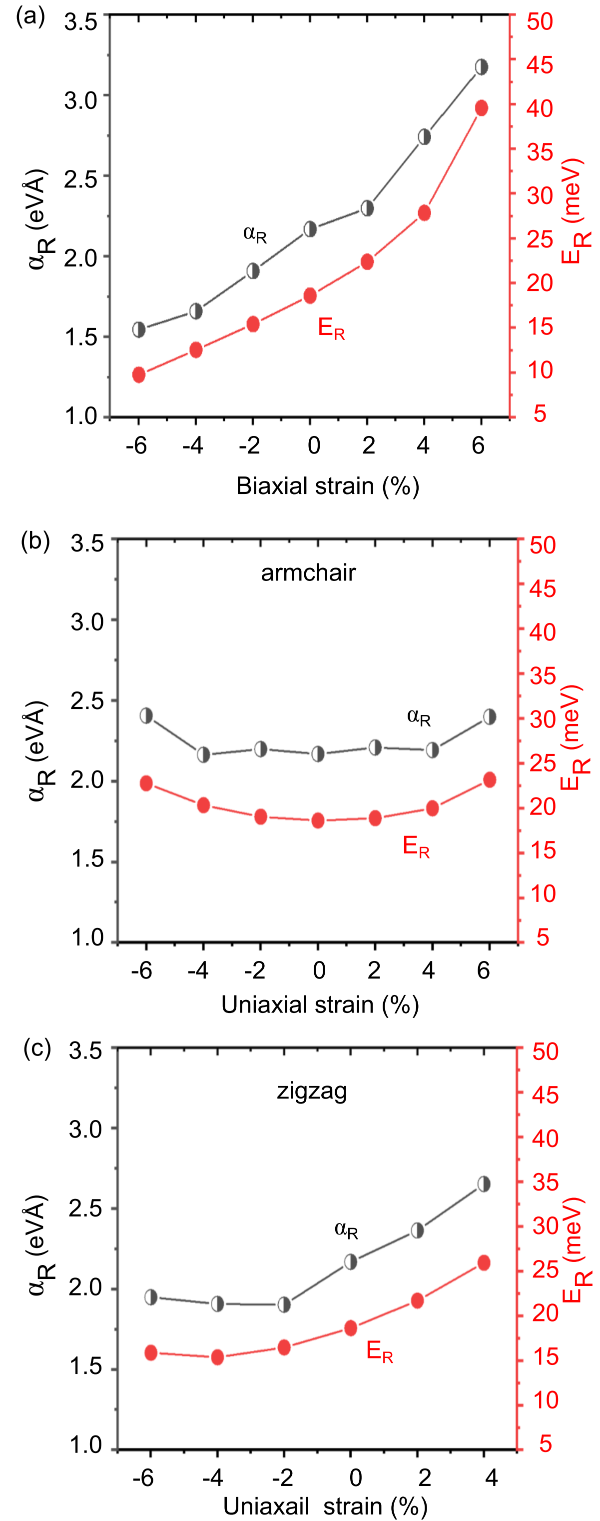

FIG. 5. Variation in Rashba parameters E_R and α_R in monolayer BiAs with (a) biaxial and uniaxial strain along the (b) armchair and (c) zigzag directions.

Dresselhaus-type SOC. The calculated Rashba energy E_R = 93 meV and the Rashba coupling constant α_R = 4.35 eV Å for the conduction band, and E_R = 137 meV and α_R = 5.93 eV Å for the valence band are large compared to other bismuth-containing materials such as BiTeI, BiTeBr, BiTeCl, and $BiAlO_3$, which fall in the ranges 7.3–100 meV and 0.39–3.8 eV Å [39–42], as listed in Table I. We attribute these to the stronger Bi contribution to the band edges, compared to these other materials. We note, however, that other materials, such as GeTe and SnTe have even larger Rashba parameters,

The shape of the spin texture in the $k_x - k_y$ plane centered around the L point is elliptical rather than circular, as expected for a pure Rashba effect, as shown in Fig. 3(h). This indicates the contribution of the Dresselhaus SOC effect, consistent with the lack of inversion symmetry in the BiAs crystal structure.

B. Structural and electronic properties of monolayer BiAs

The structure of the monolayer BiAs with the supercell dimensions and corresponding Brillouin zone is shown in Fig. 1(c). The calculated equilibrium lattice parameters are

$a = b = 3.982$ Å, with Bi-As bond length is 2.76 Å, buckling height is 1.532 Å, and the As-Bi-As angle is 92.2°.

The phonon dispersion along the high-symmetry lines in the 2D hexagonal Brillouin zone is shown in Fig. 2(b). The longitudinal acoustic (LA) and transverse acoustic (TA) represent the in-plane vibrations. The flexural acoustic (ZA) band represents out-of-plane vibrations. As in the case of bulk, it can be clearly seen that there are no negative frequencies in the phonon band structure of the BiAs monolayer, indicating that it is structurally stable. The optical and acoustic modes are well separated from each other by more than 3.0 THz (102 cm^{-1}). This value is larger than the value of 2.1 THz (70 cm^{-1}) predicted for BiSb [43], and much larger than the highest acoustic energy acoustic phonon, with important implications to heat transport under optical excitation [51].

The electronic band structure of the monolayer BiAs is shown in Fig. 4 using the PBE functional. The band structure including SOC shows a direct band gap of 0.70 eV at Γ. This contrasts with the much smaller and indirect band gap of bulk BiAs. It is also larger than that reported for monolayer BiSb (0.37 eV) [43]. Since the PBE functional tends underestimate the band gaps, we also computed the band gap using the HSE06, finding the value of 1.72 eV (without SOC) and 1.30 with SOC), compared to 1.60 eV for BiSb [43]. The conduction bands near minimum at Γ display significantly larger dispersion than the valence bands, suggesting that electrons are expected to have significantly higher mobility than holes.

The band structure of monolayer BiAs along -K−Γ−K and the corresponding spin-resolved projections [Figs. 4(c)–4(e)] show a spin splitting of the conduction band around Γ suggesting a Rashba-type SOC. The spin splitting in the conduction band is much larger than that in the valence band. By comparing the projection on S_x, S_y, and S_z, for the conduction band, we can clearly see the contributions from S_x and S_y but not S_z, which is a clear indication of a pure Rashba effect. In this case, find $E_R = 18.6$ meV and $\alpha_R = 2.17$ eV Å. The spin texture around Γ in Fig. 4(f) shows a circular shape, confirming the pure Rashba-type spin splitting in monolayer BiAs. Even though these values are smaller than the bulk values, they are quite large compared to the giant values predicted for monolayer BiSb [43].

C. Effect of uniaxial and biaxial strain on E_R and α_R in monolayer BiAs

One of the main characteristics of 2D materials is that they support large strains and can be easily stretched by placing them on textured or bent on flexible substrates, leading to regions of uniaxial or biaxial strain. To demonstrate how strain impacts the electronic structure of BiAs, we studied monolayer BiAs under biaxial and uniaxial strains. The results, displayed in Fig. 5, show that the Rashba energy E_R and the Rashba coupling constant α_R significantly increase with biaxial tensile strain, e.g., from 18.6 meV and 2.17 eV Å to 40 meV and 3.2 eV Å for 6% strain, as seen in Fig. 5(a). However, the effect of uniaxial strain on E_R and α_R, along the zigzag or armchair directions, is much less significant [Figs. 5(b) and 5(c)], due to the smaller change in the volume with a given strain value since the length of the cell dimension in the perpendicular direction is allowed to relax according to the Poisson's ratio.

IV. CONCLUSIONS

Using DFT calculations, we identified BiAs as a 2D layered semiconductor with large Rashba splitting in the bulk and monolayer forms. Bulk BiAs is predicted to be stable in the rhombohedral crystal structure like the parent Bi and As compounds. It has a narrow and indirect band gap. It shows a combination of Rashba and Dresselhaus type spin splitting around the L point of the Brillouin zone of the conventional hexagonal unit cell. Monolayer BiAs has a much larger band gap and shows a circular spin texture, characterizing a pure Rashba effect. The Rashba parameters is significantly enhanced under tensile biaxial strain. The existence of large Rashba effects in bulk and monolayer makes BiAs a promising material for spintronics.

ACKNOWLEDGMENTS

This work was supported by the National Science Foundation Award No. OIA-2217786, and the use of Bridges-2 at PSC through allocation DMR150099 from the Advanced Cyberinfrastructure Coordination Ecosystem: Services & Support (ACCESS) Program, which is supported by the National Science Foundation Grants No. 2138259, No. 2138286, No. 2138307, No. 2137603, and No. 2138296, and the DARWIN Computing System at the University of Delaware, which is supported by the NSF Grant No. 1919839. S.K. acknowledges funding from Laboratory Directed Research and Development Program (Project No. 800025) at Princeton Plasma Physics Laboratory under U.S. Department of Energy Prime Contract No. DE-AC02-09CH11466.

[1] J. D. Koralek, C. P. Weber, J. Orenstein, B. A. Bernevig, S.-C. Zhang, S. Mack, and D. Awschalom, Nature (London) **458**, 610 (2009).

[2] M. Walser, C. Reichl, W. Wegscheider, and G. Salis, Nat. Phys. **8**, 757 (2012).

[3] Y. Ohno, R. Terauchi, T. Adachi, F. Matsukura, and H. Ohno, Phys. Rev. Lett. **83**, 4196 (1999).

[4] O. Z. Karimov, G. H. John, R. T. Harley, W. H. Lau, M. E. Flatté, M. Henini, and R. Airey, Phys. Rev. Lett. **91**, 246601 (2003).

[5] G. M. Müller, M. Römer, D. Schuh, W. Wegscheider, J. Hübner, and M. Oestreich, Phys. Rev. Lett. **101**, 206601 (2008).

[6] M. Griesbeck, M. M. Glazov, E. Y. Sherman, D. Schuh, W. Wegscheider, C. Schüller, and T. Korn, Phys. Rev. B **85**, 085313 (2012).

[7] H. Ye, G. Wang, B. Liu, Z. Shi, W. Wang, C. Fontaine, A. Balocchi, T. Amand, D. Lagarde, P. Renucci *et al.*, Appl. Phys. Lett. **101**, 032104 (2012).

[8] G. Wang, A. Balocchi, D. Lagarde, C. Zhu, T. Amand, P. Renucci, Z. Shi, W. Wang, B. Liu, and X. Marie, Appl. Phys. Lett. **102**, 242408 (2013).

[9] A. Soumyanarayanan, N. Reyren, A. Fert, and C. Panagopoulos, Nature (London) **539**, 509 (2016).

[10] Y. A. Bychkov and E. I. Rashba, JETP Lett. **39**, 66 (1984).

[11] E. I. Rashba, Sov. Phys. Solid State **2**, 1109 (1960).
[12] R. Casella, Phys. Rev. Lett. **5**, 371 (1960).
[13] G. Dresselhaus, Phys. Rev. **100**, 580 (1955).
[14] M. I. D'yakonov and V. Y. Kachorovskii, Sov. Phys. Semicond. **20**, 110 (1986).
[15] S. Fang, R. Zhu, and T. Lai, Sci. Rep. **7**, 1 (2017).
[16] E. C. Ahn, npj 2D Mater. Appl. **4**, 17 (2020).
[17] J. D. Sau, R. M. Lutchyn, S. Tewari, and S. Das Sarma, Phys. Rev. Lett. **104**, 040502 (2010).
[18] J. D. Sau, S. Tewari, R. M. Lutchyn, T. D. Stanescu, and S. Das Sarma, Phys. Rev. B **82**, 214509 (2010).
[19] J. Alicea, Phys. Rev. B **81**, 125318 (2010).
[20] M. Sato and S. Fujimoto, Phys. Rev. B **79**, 094504 (2009).
[21] V. Mourik, K. Zuo, S. M. Frolov, S. Plissard, E. P. Bakkers, and L. P. Kouwenhoven, Science **336**, 1003 (2012).
[22] A. Takayama, T. Sato, S. Souma, and T. Takahashi, New J. Phys. **16**, 055004 (2014).
[23] P. Hofmann, Prog. Surf. Sci. **81**, 191 (2006).
[24] D. Hsieh, D. Qian, L. Wray, Y. Xia, Y. S. Hor, R. J. Cava, and M. Z. Hasan, Nature (London) **452**, 970 (2008).
[25] M. Z. Hasan and C. L. Kane, Rev. Mod. Phys. **82**, 3045 (2010).
[26] C.-H. Hsu, X. Zhou, T.-R. Chang, Q. Ma, N. Gedik, A. Bansil, S.-Y. Xu, H. Lin, and L. Fu, Proc. Natl. Acad. Sci. USA **116**, 13255 (2019).
[27] F. Schindler, Z. Wang, M. G. Vergniory, A. M. Cook, A. Murani, S. Sengupta, A. Y. Kasumov, R. Deblock, S. Jeon, I. Drozdov *et al.*, Nat. Phys. **14**, 918 (2018).
[28] H. Miyahara, T. Maegawa, K. Kuroda, A. Kimura, K. Miyamoto, H. Namatame, M. Taniguchi, and T. Okuda, e-J. Surf. Sci. Nanotechnol. **10**, 153 (2012).
[29] S. Singh, W. Ibarra-Hernández, I. Valencia-Jaime, G. Avendaño-Franco, and A. H. Romero, Phys. Chem. Chem. Phys. **18**, 29771 (2016).
[30] P. Hohenberg and W. Kohn, Phys. Rev. **136**, B864 (1964).
[31] W. Kohn and L. J. Sham, Phys. Rev. **140**, A1133 (1965).
[32] G. Kresse and J. Furthmüller, Phys. Rev. B **54**, 11169 (1996).
[33] G. Kresse and D. Joubert, Phys. Rev. B **59**, 1758 (1999).
[34] J. P. Perdew, K. Burke, and M. Ernzerhof, Phys. Rev. Lett. **77**, 3865 (1996).
[35] J. Heyd, G. E. Scuseria, and M. Ernzerhof, J. Chem. Phys. **118**, 8207 (2003).
[36] J. Heyd and G. E. Scuseria, J. Chem. Phys. **121**, 1187 (2004).
[37] U. Herath, P. Tavadze, X. He, E. Bousquet, S. Singh, F. Muñoz, and A. H. Romero, Comput. Phys. Commun. **251**, 107080 (2020).
[38] M. S. Bahramy, R. Arita, and N. Nagaosa, Phys. Rev. B **84**, 041202(R) (2011).
[39] K. Ishizaka, M. Bahramy, H. Murakawa, M. Sakano, T. Shimojima, T. Sonobe, K. Koizumi, S. Shin, H. Miyahara, A. Kimura *et al.*, Nat. Mater. **10**, 521 (2011).
[40] L. G. D. da Silveira, P. Barone, and S. Picozzi, Phys. Rev. B **93**, 245159 (2016).
[41] F.-X. Xiang, X.-L. Wang, M. Veldhorst, S.-X. Dou, and M. S. Fuhrer, Phys. Rev. B **92**, 035123 (2015).
[42] C. Martin, A. Suslov, S. Buvaev, A. Hebard, P. Bugnon, H. Berger, A. Magrez, and D. Tanner, Europhys. Lett. **116**, 57003 (2016).
[43] S. Singh and A. H. Romero, Phys. Rev. B **95**, 165444 (2017).
[44] M. Sakano, M. S. Bahramy, A. Katayama, T. Shimojima, H. Murakawa, Y. Kaneko, W. Malaeb, S. Shin, K. Ono, H. Kumigashira, R. Arita, N. Nagaosa, H. Y. Hwang, Y. Tokura, and K. Ishizaka, Phys. Rev. Lett. **110**, 107204 (2013).
[45] Y. M. Koroteev, G. Bihlmayer, J. E. Gayone, E. V. Chulkov, S. Blügel, P. M. Echenique, and P. Hofmann, Phys. Rev. Lett. **93**, 046403 (2004).
[46] D. Di Sante, P. Barone, A. Stroppa, K. F. Garrity, D. Vanderbilt, and S. Picozzi, Phys. Rev. Lett. **117**, 076401 (2016).
[47] S. LaShell, B. A. McDougall, and E. Jensen, Phys. Rev. Lett. **77**, 3419 (1996).
[48] D. Di Sante, P. Barone, R. Bertacco, and S. Picozzi, Adv. Mater. **25**, 509 (2013).
[49] E. Plekhanov, P. Barone, D. Di Sante, and S. Picozzi, Phys. Rev. B **90**, 161108(R) (2014).
[50] M. Kim, J. Im, A. J. Freeman, J. Ihm, and H. Jin, Proc. Natl. Acad. Sci. USA **111**, 6900 (2014).
[51] P. G. Klemens, Phys. Rev. **148**, 845 (1966).